Astron. Astrophys. 334, 188–200 (1998)

ASTRONOMY AND ASTROPHYSICS

Loop modeling of coronal X-ray spectra

V. One- and two-loop model fitting of G-type star ROSAT/PSPC spectra

R. Ventura[1], **A. Maggio**[2], **and G. Peres**[3]

[1] Osservatorio Astrofisico, Città Universitaria, V. le A. Doria 6, I-95125 Catania, Italy
[2] Osservatorio Astronomico, Piazza del Parlamento 1, I-90134 Palermo, Italy
[3] Dipartimento di Scienze Fisiche e Astronomiche, sezione di Astronomia, Piazza del Parlamento 1, 90134 Palermo, Italy

Received 11 August 1997 / Accepted 27 January 1998

Abstract. As part of a systematic study devoted to the diagnostic of solar-like coronal structures in late-type stars, we have analyzed ROSAT/PSPC X-ray spectra of eight main sequence G-type stars in the solar neighborhood. We have fitted the X-ray spectra adopting two different classes of models: the usual two-component isothermal models and the more physically meaningful hydrostatic loop models. The two-component isothermal models yield fairly acceptable χ^2 values, however they allow limited physical insight on the stellar coronal structures; on the other hand, the one-loop model fitting provides unreliable long loops, namely orders of magnitude larger than the stellar radius, in the majority of the cases studied. A more realistic physical description of the observed coronae comes from the two-loop modeling approach: two distinct classes of loops with different characteristics seem to dominate the X-ray emission of our sample of G-type stars: relatively cool loops ($T_{\max} \simeq 1.5 - 5 \times 10^6$ K) with pressures ranging from relatively low ($p_0 \simeq 2 - 10$ dyn cm^{-2}) to high values ($p_0 \simeq 100$ dyn cm^{-2}) and hot loops ($T_{\max} \simeq 1 - 3 \times 10^7$) with very high base pressures ($p_0 \simeq 10^2 - 2.4 \times 10^4$ dyn cm^{-2}). We compare the results and the diagnostic power coming from the different approaches and discuss their physical implications.

Key words: stars: coronae – stars: late-type – stars: activity – plasmas – X-rays: stars

1. Introduction

In spite of the wealth of spectral data so far collected in decades of stellar X-ray observations, until now the standard analysis of X-ray spectra of stellar coronae has been to fit the observations with models characterized by one, or at most two, optically thin plasma components at different temperatures (e.g. White et al. 1994, Drake et al. 1994). This kind of approach, certainly supported by the well established thermal nature of the X-ray stellar emission, however allows the estimation of only a sort of "average" value of the emitting coronal plasma temperature distribution, weighted through the instrumental spectral response, and by the relative weight of the plasma at different temperatures.

Albeit the one- and two-component isothermal models (hereafter 1-T and 2-T models) were quite appropriate to the analysis of the coarse *Einstein* Observatory Imaging Proportional Counter (IPC) spectra, they may provide a too limited interpretation of the more detailed ROSAT Position Sensitive Proportional Counter (PSPC) data and, a fortiori, of the very detailed spectra which will be collected by XMM and AXAF. Another shortcoming of such a model is the limited insight into coronal physical conditions which, in the best studied case, the Sun, show a more complex structuring: the entirety of the EUV and X-ray emission (ranging from quiet to very active regions) comes from coronal loops, i.e. hot plasma magnetically confined in arch-like structures, with temperature stratification within each loop and a temperature diversification among different loops (see Linsky & Serio, 1993). In practice, each loop – characterized by different physical parameters such as temperature, pressure and length – is a mini-corona by itself (Rosner et al. 1978), being thermally and dynamically independent from the others.

In the past, some work has already been devoted to loop modeling of stellar coronae but only one-loop models were adopted (Schmitt et al. 1985, Giampapa et al. 1985, Landini et al. 1985, Stern et al. 1986, Schrijver et al. 1989, Ottmann 1993). In principle, this assumption seems to be supported by several theoretical and observational studies performed in this context: even though one observes a distribution of loops, a single class of them, namely the hottest and densest ones, may dominate the disk-integrated stellar X-ray emission (e.g. Antiochos & Noci 1986; Ciaravella et al. 1996, hereafter Paper I). Nevertheless, as pointed out by extensive simulations of X-ray spectra (Maggio & Peres 1996, hereafter Paper II) and the results of the analysis performed on real X-ray observations (Maggio & Peres 1997a, hereafter Paper IV), in some cases the one-loop model fails to fit the data and a two-loop model fitting appears to work better.

The state of the art, as depicted above, is very puzzling and incomplete, hinting at the need of systematic and accurate studies on the matter. This work is part of a wide project aimed at investigating the analysis of stellar coronal X-ray spectra in

Send offprint requests to: rventura@alpha4.ct.astro.it

terms of 2-T models and loop models (also comparing their diagnostic properties), and at the application of loop modeling to fit real X-ray data (Paper I; Paper II; Ciaravella et al. 1997, hereafter Paper III; Paper IV). The scope of the present work is to perform an accurate analysis on a well-chosen sample of G-type dwarfs and to sound the influence of stellar age on the coronal structures. With this perspective we apply 2-T models and loop-models to ROSAT/PSPC observations of a selected sample of nearby solar-like stars. Another paper of the series carries out a similar analysis on F-type stars (Maggio et al. 1997c, hereafter Paper VI) allowing, in perspective, comparison also of the coronal properties for stars of different spectral types.

The paper is organized as follows: in Sect. 2 we report the criteria adopted in selecting the sample; in Sect. 3 we described the data analysis and discuss the results and in Sect. 4 we draw some conclusion.

2. The star sample

The sample of stars has been selected as follows:

1. we first selected all X-ray sources both present in the Max Planck Institut für Extraterrestrische Physik (MPE) ROSAT/PSPC catalogue (Voges et al. 1994) and identified with main sequence G stars (either single or binary system components) in the Third Catalog of Nearby Stars (CNS3, preliminary version; Gliese & Jahreiss 1991), which reports stars within 25 pc from the Sun;
2. we then selected only observations with more than 800 total counts in order to ensure sufficient photon counting statistics;
3. for the sake of sample homogeneity we discarded all known RS CVn-type binaries, except the *suspected* RS CVn system component GJ 566A;
4. stars whose spectra might have been perturbed by the proximity to the support structure of the PSPC entrance window were also rejected.

The final sample of eight stars is given in Table 1, which also provides information on their optical properties, multiplicity, distance, age and rotational period.

Two stars in our sample, GJ 559A and GJ 566A, are part of a binary system and in both cases the two components of the pair are potential X-ray sources. In the case of the system GJ 559, X-ray observations performed at high angular resolution with the High Resolution Imager (HRI) on board *Einstein* showed that about 70% of the total X-ray emission can be attributed to the B component of the pair, a K1V type star (Golub et al. 1982). Nevertheless we decided to include the target in our sample all the same as an interesting case, because it is intermediate between G and K type stars.

The only X-ray observations at high angular resolution of GJ 566, known to the authors, are those performed with the High Resolution Imager (HRI) on board ROSAT (Walter, 1982). Even if the two components of the system are unresolved, on the basis of the inspection of the ROSAT/HRI images, Schmitt (1997) deduces that most of the X-ray emission comes from only one component, presumably the optical primary. Following Schmitt we attribute the total X-ray emission to the G8V component of the pair.

3. Data analysis

The source and background spectrum extraction was carried out by the Post-Reduction Off-line Software (PROS V 2.4) running under the Image Reduction and Analysis Facility (IRAF V 2.10) software, while the spectral fitting was performed with the Analysis System for Astrophysical Plasmas (ASAP V 3; Maggio et al. 1994).

Table 2 summarizes the characteristics of the X-ray observations obtained from the analysis with PROS of the X-ray images, together with the derived values of X-ray fluxes and luminosities.

As reported in Table 2 the observational sequence WG 201119 (hereafter briefly identified by the symbol #1) of the binary star GJ 559 was split into three different time intervals (OBI) yielding not more than about 6000 total source counts. We have selected this photon count threshold in order to reduce the influence of systematic errors, due in practice to the present calibration uncertainties in the PSPC energy response: at high counting statistics such systematic errors might dominate the fitting results (see Bocchino et al. 1994 for a detailed analysis of the topic). WG180025, the other observational sequence of the binary star GJ 559, is about one year apart from the sequence #1; hereafter it will be identified by the symbol #2. Analogously, the two observational sequences of the star GJ 620.1, more than one year apart, hereafter will be identified by the symbols #1 and #2.

Since we are interested in the emission of *steady* coronal structures, a preliminary search for variability was performed using the Kolmogorov - Smirnov and the Cramer - Von Mises statistical tests available in PROS. No significant variability, i.e. with confidence level larger than 99%, was detected for any of the stars except for GJ 566 (the *suspected* RS-CVn system) for which both tests indicate significant variability at the 99% confidence level. No flares are evident in the light curve of the star.

For each star the search for variability was also applied to the soft and hard bands of ROSAT/PSPC separately, in order to investigate if some variability was present only in one of the two spectral bands (0.1 -0.4 keV and 0.4 - 2.4 keV) and blurred in the total energy band. In the case of the stars GJ 502 both tests detect significant variability in the hard energy band light curve with a 99% confidence level and no variability in the total energy band nor in the soft one.

The implications of these results will be discussed later.

For the spectral analysis of the PSPC spectra we have adopted the appropriate post-launch calibration response matrix, namely dtmat_36.ieee; only for GJ 566 we have used the response matrix dtmat_6.ieee because it was observed before October 1991 (Briel et al. 1996). In the fitting procedure we have excluded the first two pulse-independent (PI) spectral bins (0.07 - 0.11 keV), according to the standard 34 bins scheme,

Table 1. Optical properties of the target stars

Name	Other name	Spectral Type	m_v	B-V	Distance (pc)	Age (10^9 yr)	$v \sin i$ (km s^{-1})	$P_{\rm rot}$ (days)
GJ 17.3	BE Cet	G2V	6.4	0.66	20.4 ± 2.30	0.6[a]	7.0 ± 0.8[e]	7.65[a]
GJ 311	π^1 Uma	G1.5 Vb	5.6	0.62	13.9 ± 1.40	0.3[a]	9.5 ± 0.6[f]	4.68[a]
GJ 502	β Com	G0V	4.3	0.58	8.30 ± 0.50	1.6[a]	4.3 ± 0.6[f]	12.4[a]
GJ 534	η Boo	G0IV	2.7	0.58	9.52 ± 0.67	2.3[b]	13.0 ± 1.0[g]	11[l]
GJ 559	α Cen	G2V + K1V	0.0	0.68	1.30 ± 0.03	5-6[a]	2.7 ± 0.7[e]	~ 30[a]
GJ 566	ξ Boo	G8V + K4V	4.7	0.72	6.70 ± 0.20		2.7 ± 0.6[h]	6.31[m]
GJ 620.1	HR 6094	G5V	5.4	0.62	14.86 ± 1.5	0.3[c]	1.4 ± 0.5[e]	8.5[e]
GJ 732.1	HR 7123	G9IVa	5.5	0.84	24.39 ± 2.6	4.0[d]	1.0 ± 1.0[i]	

a) Güdel et al. 1997; b) Guenther & Demarque, 1996; c) Porto de Mello & Da Silva, 1997; d) Schaller et al., 1992; e) Saar & Osten, 1997; f) Soderblom & Mayor, 1983; g) De Medeiros et al., 1997; h) Gray, 1984; i) De Medeiros 1997 - priv. comm.; l) lower limit from v sini; m) Donahue et al., 1996.

Table 2. X-ray observation summary

Name	Sequence	Off-axis [a] (arcmin)	ΔR[b] (arcmin)	Livetime [c] (sec)	Count Rate (counts s^{-1})	log $F_{\rm x}$ (erg cm^{-2} s^{-1})	log $L_{\rm x}$ (erg s^{-1})
GJ 17.3	US201470	0.3	0.06	5488	0.404 ± 0.008	6.32	29.10
GJ 311	US201472	0.1	0.08	4988	0.863 ± 0.013	6.28	29.06
GJ 502	US201471	0.2	0.12	8374	0.355 ± 0.006	5.28	28.12
GJ 534	US700392	19.3	0.18	11553	0.147 ± 0.004	4.32	27.99
GJ 559	WG201119	0.6	1.46[d]	3323			
(OBI1)				1343	5.142 ± 0.062	4.62[e]	27.58
(OBI2)				1218	4.714 ± 0.062	4.55[e]	27.51
(OBI3)				762	4.657 ± 0.078	4.55[e]	27.52
	WG180025	0.3	1.60[d]	374	9.880 ± 0.162	4.99[e]	27.95
GJ 566	CA150090	0.1	0.09	533	2.319 ± 0.066	6.34[e]	28.81
GJ 620.1	WG200588	5.4	0.26	1875	0.708 ± 0.019	6.33	29.05
	WG200588P-1	5.4	0.14	1316	0.784 ± 0.024	6.33	29.06
GJ 732.1	US200976	0.3	0.06	1903	0.903 ± 0.022	6.03	29.69

[a] off-axis angle; distance between the X-ray source and the PSPC field center

[b] distance between the X-ray and the optical positions of the program stars

[c] Average lifetime over the source region, computed from the exposure map

[d] This high value may be determined by an inadequate correction for the star high proper motion

[e] for the whole binary system

because of uncertainties in the instrumental response that may lead to systematic errors. Moreover we have excluded those few bins with less than 5 counts/bin, because they do not contribute properly to the χ^2 statistics (for more details on this point see Paper IV).

3.1. Isothermal models

All the stars in the sample were fitted with the ASAP procedure both with 1-T and with 2-T models of an optically-thin plasma (Raymond & Smith 1977; Raymond 1991 - priv. comm.) with solar abundances and in conditions of ionization equilibrium. The interstellar absorption model from Morrison & McCammon (1983) was also adopted, assuming an hydrogen column density, N_H, determined on the basis of the stellar distance and assuming an hydrogen number density of 0.07 cm^{-3}, suitable for the sample of stars here considered, all in the solar neighborhood (D$<$ 25 pc).

All the stars were poorly fitted with the 1-T model, leading to unacceptably large χ^2 values; for this reason we do not describe 1-T fits in detail. In the case of the 2-T model we considered four free parameters, namely two temperatures T_1 and T_2, and two emission measures, EM_1 and EM_2 ($EM = \int n_e^2\, dV$) and kept N_H fixed to the value obtained as above. As a measure of the goodness-of-fit, in Table 3 we report the reduced χ^2 values together with the best fit values of the parameters of interest. The adopted absorption column density for each star is also reported.

The model fits invariably provide acceptable or, sometimes, marginally acceptable χ^2 for all the spectra examined, except for the sequence #2 of the star GJ 559. In Fig. 1 we report, as representative examples, the χ^2 contour plots, showing the joint confidence levels (at 90%) on the model parameters of interest,

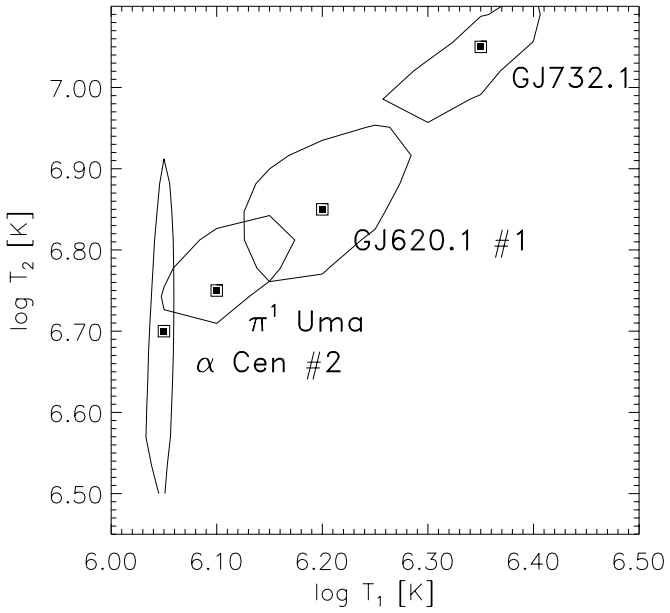

Fig. 1. 2-T model fitting. 90% confidence regions in the T_1 - T_2 plane for the stars GJ 559 (α Cen) #1 OBI2, GJ 311 (π^1 UMa), GJ 620.1 #1 and GJ 732.1, shown as examples of the solutions obtained. The squares indicate the best fit values of T_1 and T_2.

defined according to Avni (1976), for some of the fits obtained. The general trend, shared by all our sample except the stars GJ 502 and GJ 559 #2, is an increase of both temperatures with increasing emission levels.

The results obtained can be grouped in, at least, three different classes of solutions with different characteristics.

At one extreme, the spectra of the three segments of the star GJ 559 (#1) are quite soft and dominated by a very well constrained low-temperature component $T_1 = 1.0 \times 10^6$ K while the higher temperature component is poorly constrained by the fitting. In Fig. 1 we show the results relevant to the segment GJ 559 #1, OBI2; the other two segments, OBI1 and OBI3, yield very similar results. The contribution of the cool component to the total emission measure is more than 79% in each OBI.

At the other extreme, for GJ 311 (π^1 UMa) and GJ 732.1, the low and high temperatures are both very well constrained by the fitting (Fig. 1) and the coronal emission measure is somewhat dominated by the hot component ($EM_2/EM_1 \simeq 1.4$). In passing we note that the very high best-fit value of T_2 for the star GJ 732.1 ($T_2 = 1.1 \times 10^7$ K) is very near the threshold of the instrumental sensitivity.

The spectra of all the other stars have intermediate characteristics (see for instance GJ 620.1 in Fig. 1): the two temperatures are constrained by the fitting to the same extent, with different levels of discrimination from star to star, and depending on the photon counting statistics; typically the emission measure of the low temperature component, namely EM_1, dominates the spectrum but a significant contribution comes also from EM_2.

Although the model fits described above provide good formal fits to the data, the derived parameters are not easy to interpret from the physical point of view.

A common but questionable assumption, often used in literature (see for example Giampapa et al. 1996) is that *each* isothermal component derived by the 2-T fitting can be identified with *one* class of loops dominating the emission of the stellar coronae. However at least two different considerations may weaken this explanation: (a) the loop structures observed in X-rays on the Sun do not show evidence of isothermal temperature distributions (Kano & Tsuneta 1995, 1996), and (b) the simulations presented in Paper III show that in some cases the synthesized spectra for a model corona dominated by only one class of loops are well fitted by the 2-T model, but not always with the 1-T model. Therefore a 2-T fitting does not grant certain presence of two dominating classes of loops on the star, and make it uncertain the determination of the relevant thermodynamic properties of the coronal structures. Such considerations lead to a demand for fitting the data with detailed loop model spectra.

3.2. One-loop models

We have proceeded in our analysis, on the hypothesis that the X-ray stellar emission can be explained (as commonly accepted) in terms of loop emission, and with the assumption, as a first step, that a single class of them, all with identical characteristics, dominates the X-ray emission.

We adopted the hydrostatic loop model based on the numerical code developed by Serio et al. (1981) with the enhancements reported in Paper I. The model describes the coronal plasma as a fluid in hydrostatic equilibrium under the effect of gravity and with steady energy balance between a uniform heating, optically thin radiative losses and thermal conduction. The plasma is magnetically confined inside semicircular loop-like structures, mirror symmetric with respect to their apex and with constant (or optionally expanding) loop cross-section. In the present case we restricted our attention to loops with constant cross section, a hypothesis supported by the observations made with the soft X-ray solar telescopes on Skylab and YOHKOH, showing that the majority of compact and more intensely emitting loops have nearly constant cross sections along their lengths, rather than expanding with height (Klimchuk et al. 1992). The static approximation adopted is consistent with a scenario in which the X-ray emitting structures of interest are observed to be relatively quiescent, i.e. change very little on the characteristic dynamic and thermodynamic time scales of the plasma evolution.

In the adopted model each loop configuration is uniquely characterized by two of the following three parameters, linked together by the Serio et al. (1981) scaling law: the semi-length L, the plasma pressure p_0 at the base of the transition region, and the plasma maximum temperature $T_{\max}$, at loop apex. The third free parameter of the loop model is a normalization factor which depends on the surface filling factor f, i.e. the fraction of the stellar surface covered by the loop footpoints, and on the fraction of the X-ray emitting volume obscured by the stellar disk.

Following the analysis described in Paper II and IV, in order to search for the best fit model, we adopted a *grid* of 50 x 20

Table 3. Two-temperature model fits

Name	Counts	Chans[a]	log $N_{\rm H}$ ($\rm cm^{-2}$)	T_1 (10^6 K)	90% conf. range[b]	T_2 (10^6 K)	90% conf. range[b]	EM_2/EM_1	$\chi^2_{\rm red}$
GJ 17.3	2164 ± 52	3:27	18.65	1.58	1.41 - 2.00	6.31	> 5.01	0.96	0.6
GJ 311	4211 ± 70	3:28	18.48	1.26	1.12 - 1.41	5.62	5.62 - 6.31	1.37	1.2
GJ 502	2875 ± 59	3:22	18.25	1.26	1.12 - 1.26	3.55	2.82 - 4.47	0.41	0.8
GJ 534	1637 ± 48	3:23	18.31	1.58	1.41 - 1.78	5.01	> 3.16	0.41	0.7
GJ 559 #1									
(OBI1)	6569 ± 85	3:23	17.46	1.00	1.00 - 1.12	3.55	3.16 - 5.62	0.26	1.4
(OBI2)	5423 ± 62	3:21	17.46	1.12	1.12 - 1.12	5.01	> 3.16	0.07	1.0
(OBI3)	3347 ± 62	3:20	17.46	1.12	1.12 - 1.12	4.47	> 2.82	0.10	1.0
GJ 559 #2	3554 ± 65	3:28	17.46	1.12	1.12 - 1.26	7.94	> 7.08	0.49	1.9
GJ 566	1152 ± 39	3:26	18.16	1.26	1.00 - 1.58	5.01	5.10 - 5.12	1.18	0.6
GJ 620.1									
#1	1293 ± 43	3:26	18.51	1.58	1.41 - 1.78	7.08	6.31 - 8.91	0.79	0.7
#2	996 ± 37	3:25	18.51	1.26	1.12 - 1.58	6.31	> 4.47	0.94	0.4
GJ 732.1	1677 ± 46	3:27	18.72	2.24	2.00 - 2.50	11.20	10.00 - 12.6	1.50	0.9

[a] Range of energy bins used among the 34 available

[b] In some cases the best fit is equal to one of the range boundaries because of the finite resolution of the model grid used for the χ^2 fitting

models in the $T_{\rm max}$ - L parameter space spanning, at equal steps in the logarithm, the ranges log $T_{\rm max}$ (K) = [6.0 - 7.47] and log L (cm) = [8.15 - 12.9]. The normalization factor has been computed analytically, for each grid model, by minimizing the χ^2 value.

The adopted values of stellar radius and mass, required to compute the loop models, are those reported in Allen (1973) for each spectral type and luminosity class; we have used more accurate and specific estimates of them, available in literature, for GJ 534 (Harrington et al. 1993), GJ 559A (Demarque et al. 1986, Soderblom 1986) and GJ 732.1 (Güdel et al. 1995). It is worth noting that for GJ 559, a binary system, we have tested that the results of the fittings do not depend significantly on which of the two stars is assumed to be the X-ray source; identical considerations hold for the two-loop fitting, the subject of the next section.

The results of the one-loop fitting are reported in Table 4. Except for the star GJ 559 ($\chi^2_{\rm red}$ in the range 2.0 - 3.4), we have obtained either good fits ($\chi^2_{\rm red} < 1$) or marginally good fits ($\chi^2_{\rm red} \leq 1.3$). Nevertheless for all but GJ 534 we obtain values of L, the semi-length of the loop, orders of magnitude larger than the stellar radius thus making the hydrostatic loop assumption unreliable, since the loop sound-crossing time is very large.

In the two top panels of Fig. 2 we report the confidence region in the p_0 - L and $T_{\rm max}$ - L planes for GJ 534, namely the only physically acceptable case. Since the spectrum is best-fitted by short loops, shorter than one pressure scale height $s_{\rm p}$, the maximum temperature is very well constrained (log $T_{\rm max}$ = 6.5 - 6.8) while the two other significant parameters p_0 and L are not constrained separately, due to the scale invariance of the equations describing the hydrostatic model of uniform pressure (see Paper II and Paper IV).

As an example of the one-loop fitting results obtained for all the other stars, in Fig. 2 (bottom panels) we show the confidence regions traced in the p_0 - L and $T_{\rm max}$ - L planes obtained for the star GJ 17.3. The base pressure of the best-fit one-loop model is well constrained between the values 2.52 - 3.25 dyn $\rm cm^{-2}$, while only lower limits can be obtained for L and $T_{\rm max}$: respectively log $L > 10.6$ and log $T_{\rm max} > 6.8$. For $L > s_{\rm p}$ our inability to fix upper limits on L and $T_{\rm max}$ comes from two distinct factors: the observed spectrum is not very sensitive to a further increase of L since the high-temperature plasma near the loop apex contributes weakly to the emission measure (see Paper IV) and the high value of $T_{\rm max}$ is outside the instrument spectral sensitivity. As already discussed in Paper IV, we decided to reject this kind of solutions because high values of L, orders of magnitude greater than the stellar radius, are physically unacceptable.

3.3. Two-loop models

Since the one-loop model yields unreliable fitting results for all the stars analyzed except GJ 534, we decided to apply the more complex two-loop model fitting to the complete sample of G stars, then including also the star GJ 534, in order to search for a physically more realistic description of the data.

The search for the best-fit solutions and the exploration of the six-dimensional parameters space, as well as the construction and visualization of statistical confidence regions, are described in details in Paper IV. Table 5 reports the results of the 2-loop model fitting: the best fit values of the parameters of interest, the corresponding 90% confidence ranges, the relevant X-ray luminosities and the reduced χ^2 values are shown for each of the two-loops components.

The solutions obtained are in all cases acceptable or marginally acceptable, including the case of GJ 559 (#2), which was the only one poorly fitted by the 2-T model. As representative examples of the solutions obtained, in Fig. 3 we show the observed PSPC spectra, the two-loop best-fit models and the fit residuals for the stars GJ 559 (#1 OBI2 and #2), GJ 311 (π^1 UMa) and GJ 732.1. In Figs. 4 and 5 we show the 90% confi-

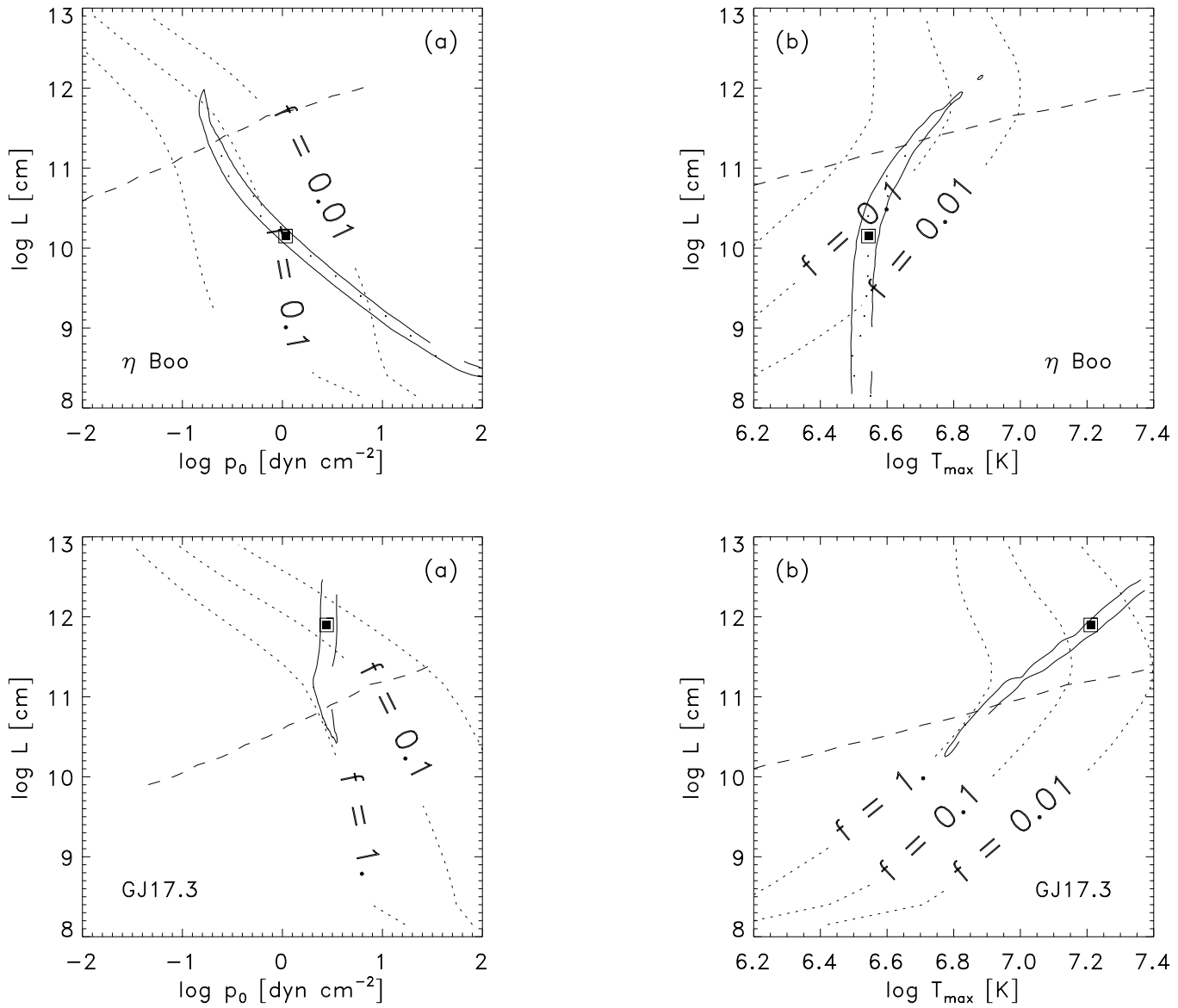

Fig. 2a and b. One-loop solutions. Top panels: confidence regions at the 90% level in the p_0 - L (**a**) and in the $T_{\max}$ - L (**b**) parameter spaces for GJ 534 (η Boo). Bottom Panels: the same as top panels but for GJ 17.3. The squares show the global best-fit loop model parameter values. Dotted lines mark different contour levels of total filling factor; the dashed lines mark the locus where the height of the loop H, is equal to the pressure scale height, $s_{\rm p}$, at $T = T_{\max}$.

dence regions in the loop parameter space for GJ 559 (#1 OBI2) and GJ 311, respectively.

In the case of GJ 559 (#1 OBI2), close inspection of Fig. 4 (middle row of figures) indicates that the constraint on the total filling factor, $f_1 + f_2 < 1$, allows by itself to put an upper limit on the loop length and hence a stringent constraint on the low $T_{\max}$, from which also a lower limit on the plasma pressure at the loop base can be derived. In all the other cases (see as an example Fig. 5) the $f_1 + f_2 < 1$ condition is not sufficient to constrain the low-$T_{\max}$ loop length and two scenarios are possible: loops shorter than the pressure scale height ($s_{\rm p} \simeq 5 \times 10^3 \times T_{\max}\, g_\odot/g_\star$ [cm]), or very long loops. We consider the latter solutions much less physically realistic, so we concentrated our attention only on the short loop solutions, for which the same constraints on $T_{\max}$ and p_0, described for the case of GJ 559, hold.

For the high-$T_{\max}$ loop components we can usually put firm lower limits on $T_{\max}$, while an upper limit cannot be fixed in general. If we again restrict our attention only to solutions with high-$T_{\max}$ loops shorter than the pressure scale height, we are able to find an upper constraint on $T_{\max}$, and to put a lower limit on p_0 for GJ 311, GJ 502, GJ 559 #1 OBI1 and GJ 559 #2. This is not possible in all the other cases because of the limited sensitivity of the PSPC to plasma components at temperatures higher than a few 10^7 K. The confidence ranges reported in Table

Table 4. One - loop model fitting results

Name	p_0 dyne cm^{-2}	90% conf. range	L 10^{10} cm	90% conf. range	$T_{\max}$ 10^6 K	90% conf. range	f	90% conf. range	$\chi_{\rm red}$
GJ 17.3	2.76	2.52 - 3.25	79.1	> 4.46	16.3	> 6.83	0.04	< 0.92	0.9
GJ 311	2.76	2.52 - 3.03	79.1	> 25.0	16.3	> 11.3	0.04	< 0.26	1.0
GJ 502	0.53	0.48 - 0.71	79.4	> 1.41	8.95	> 2.99	0.08	< 1.74	1.3
GJ 534	1.08	> 0.15	1.41	< 79.2	3.50	3.14 - 6.42	0.06	< 0.20	1.3
GJ 559									
#1									
(OBI1)	0.32	0.32 - 0.32	446	> 446	12.3	> 12.3	0.00		2.4
(OBI2)	0.21	0.21 - 0.36	446	> 79.4	10.6	> 1.97	0.00		2.5
(OBI3)	0.25	0.22 - 0.36	251	> 0.79	9.50	> 1.97	0.01		2.0
#2	0.87	0.74 - 0.96	251	> 251	14.9	> 14.9	0.00		3.4
GJ 566	2.00	1.55 - 2.35	250	> 7.93	20.1	> 7.71	0.00	< 0.66	0.7
GJ 620.1									
#1	2.35	1.96 - 3.25	141	> 7.93	18.0	> 7.70	0.02	< 0.92	1.4
#2	2.00	1.67 - 276	251	> 14.1	20.1	> 8.70	0.01	< 0.87	0.6
GJ 732.1	0.63	0.63 - 0.96	793	> 446	21.0	> 18.8	0.01	< 0.01	1.3

In the cases of bad fits (χ^2 in the range 2.0 – 3.4) the 90% confidence range of f is not reported because not computed.

5 have been computed assuming that the condition $H < s_{\rm p}$ is always satisfied.

It is certainly worth trying a comparison of our results with what known of the solar corona. To this end in Fig. 6 we have reported the X-ray surface fluxes, computed for each star and for each loop component of the two-loop model, vs. the best-fit values of $T_{\max}$ and p_0, together with indicative values for the quiet and active Sun[1].

Different levels of activity characterize our sample of solar-like stars, as indicated by an evident spread in the values of X-ray surface fluxes, ranging from those typical for solar active regions to very high values. The fractional contribution of each loop component to the total average flux may differ significantly from star to star but there is a trend of higher and higher contribution from the hotter loop component with increasing activity level.

The low-$T_{\max}$ loops have $T_{\max}$ ranging from values typical of the solar quiet regions ($\simeq 1.5 \times 10^6$ K), to values typical of solar active region cores (5×10^6 K) and base pressure comparable to, or higher, than those in solar active regions ($p_0 \simeq 2 - 100$ dyn cm^{-2}). A selection effect may be responsible for the lack of low-pressure loops: they are very low emitters and hence hard to observe with the sensitivity of ROSAT/PSPC observations (cf. also Paper I). In passing, we note that the stars with the lowest surface X-ray fluxes and the lowest loop base pressure are GJ 559 (α Cen) #1 and GJ 534.

High-$T_{\max}$ loops tend to have both $T_{\max}$ and p_0 larger than in the solar active regions, with the best-fit temperatures and pressures comparable, in many cases, to values found in solar flaring loops ($T_{\max} \simeq 1 - 3 \times 10^7$ K and $p_0 \simeq 10^2$ - 10^3 dyn cm^{-2}). Again GJ 559 (α Cen) #1 and GJ 534 are the only cases in which the high-$T_{\max}$ component provides a relatively minor contribution to the spectrum according to their relatively low activity level, while the low-$T_{\max}$ and the high-$T_{\max}$ loop components of GJ 559 (α Cen) #2 have nearly comparable fluxes.

A significant insight on these results may come from the analysis of the volume emission measure (VEM) distribution vs. temperature, derived from the best-fit two-loop model for each star of our sample, which gives us a more complete description of the amount of coronal plasma at different temperature contributing to the X-ray emission. In the top panel of Fig. 7 we show the VEM distributions (integrated in constant bins with $\Delta \log T = 0.1$), for a representative set of stars of our sample. In the bottom panel of the same figure the VEM distributions for the time intervals #1 and #2 of the star GJ 559 (α Cen) are also reported.

The shape of the VEM of each star is given by the superposition of each loop component contribution, with two pronounced maxima around the corresponding maximum temperatures (see Serio et al. 1981 for details), and with a minimum in between which tends to shift slightly toward lower temperatures with stellar age because the low-$T_{\max}$ loop component tends to be cooler for older stars. For the same reason, the general trend, shared by all the stars of our sample except GJ 732.1, is a decrease of the total amount of the VEM with decreasing X-ray luminosity and age, with the most dramatic fall occurring in the emission measure of the high-$T_{\max}$ loop component, because of the decrease of the contribution of the coronal plasma at temperatures higher than about 10^4 K, and a more rapid depletion of plasma at temperatures higher than 10^7 K.

As already mentioned, only the star GJ 732.1 seems to deviate from the trend outlined before: it shows the highest X-

[1] Assuming that the quiet Sun can be modeled with loops having $\log T_{\max} = 6.25$, $p_0 = 0.1$ dyn cm^{-2}, $L = 2 \times 10^{10}$ cm, covering 50% of the Sun surface, and the active Sun with loops having $\log T_{\max} = 6.7$, $p_0 = 5$ dyn cm^{-2}, L$= 10^{10}$ cm, covering 1% of the Sun surface (Mewe 1991, and references therein), we have computed the corresponding X-ray luminosities, which are respectively $L_{\rm x} = 1.5 \times 10^{26}$ erg s^{-1} and $L_{\rm x} = 2 \times 10^{27}$ erg s^{-1}, in the 0.1 - 2.4 keV band.

Table 5. Two-loop modeling results

	Low-T_{max} components										
Name	T_{max}	90% conf	p_0	90% conf	L	90% conf	f	90% conf	L_x	90% conf	
	10^6 K	range	dyn cm^{-2}	range	10^9 cm	range		range	10^{27} erg s^{-1}	range	
GJ 17.3	5.3	1.1 - 6.0	4.	> 1.1	14.1	< 25.1	6.7e-01	< 1.0	95.0	4.3 - 110.	
GJ 311	2.1	1.2– 6.0	26.	> 2.1	0.2	< 25.1	1.2e-01	< 1.0	34.0	14. - 100.	
GJ 502	1.8	1.2 - 2.4	17.	> 0.8	0.2	< 4.5	5.9e-02	< 1.0	9.3	2.3 - 13.	
GJ 534	2.9	0.5 - 4.0	7.	> 0.02	1.4	< 79.4	9.5e-03	< 1.0	8.3	0.0 - 10.	
GJ 559 #1											
OBI1	1.4	1.3 - 1.6	2.	> 0.9	0.8	< 1.4	5.3e-01	< 1.0	3.4	2.8 - 3.6	
OBI2	1.4	1.3 - 1.6	2.	> 0.9	0.8	< 1.4	5.2e-01	< 1.0	3.3	2.9 - 3.5	
OBI3	1.5	1.3 - 1.7	110.	> 0.8	0.1	< 2.5	6.6e-03	< 1.0	3.3	2.6 - 3.5	
GJ 559 #2	1.5	1.3 - 2.0	110.	> 1.2	0.1	< 2.5	9.8e-03	< 0.8	5.0	4.4 - 5.9	
GJ 566	2.0	0.7 - 5.3	250.	> 1.3	0.1	< 14.1	1.3e-02	< 1.0	19.0	0.0 - 59.	
GJ 620.1 #1	2.1	1.3 - 5.3	26.	> 3.4	0.2	< 14.1	1.5e-01	< 1.0	36.0	13. - 88.	
GJ 620.1 #2	1.8	0.9 - 4.6	17.	> 3.6	0.2	< 7.9	3.1e-01	< 1.0	38.0	7.3 - 100.	
GJ 732.1	3.5	1.6 - 6.0	1300.	> 0.6	0.1	< 141.1	7.0e-04	< 1.0	130.0	46.0 - 190.	

	High-T_{max} components										
	T_{max}	90% conf	p_0	90% conf	L	90% conf	f	90% conf	L_x	90% conf	χ^2_{red}
	10^6 K	range	dyn cm^{-2}	range	10^9 cm	range		range	10^{27} erg s^{-1}	range	
GJ 17.3	27.2	> 5.5	96.	> 3.2	79.2	< 79.4	7.9e-04	< 0.6	34.0	16. - 120.	0.9
GJ 311	8.4	6.8 - 27.4	1700.	> 6.2	0.2	< 79.4	7.9e-04	< 0.2	91.0	27. - 110.	1.1
GJ 502	5.1	3.0 - 27.4	66.	> 1.1	0.8	< 79.4	1.9e-03	< 0.6	4.4	1.3 - 12.	1.1
GJ 534	27.2	> 3.2	17.	> 0.2	445.8	< 445.8	1.7e-05	< 0.1	2.1	0.0 - 10.	1.3
GJ 559 #1											
OBI1	6.4	4.1 - 13.8	730.	> 2.5	0.2	< 44.6	3.5e-05	< 0.03	0.8	0.7 - 1.4	1.5
OBI2	8.2	> 3.4	16000.	> 1.6	0.1	< 79.2	4.7e-07	< 0.03	0.3	0.2 - 0.7	1.2
OBI3	10.0	> 3.1	530.	> 1.1	0.8	< 79.2	1.3e-05	< 0.08	0.4	0.3 - 1.0	1.2
GJ 559 #2	12.1	8.7 - 20.8	80.	> 9.4	7.9	< 79.1	8.7e-04	< 0.01	5.0	4.3 - 5.5	1.5
GJ 566	7.3	> 4.6	1100.	> 3.7	0.2	< 79.2	1.1e-03	< 0.68	39.0	0.0 - 59.	0.7
GJ 620.1 #1	9.3	> 6.2	24000.	> 4.8	0.1	< 79.4	5.5e-05	< 0.37	78.0	30. - 96.	1.4
GJ 620.1 #2	8.4	> 5.2	1700.	> 3.2	0.2	< 79.4	9-2e-04	< 0.86	84.0	29. - 110.	0.5
GJ 732.1	27.4	> 13.8	960.	> 5.8	7.9	< 445.8	3.5e-04	< 0.02	330.0	260. - 400.	1.0

ray emission level and the hardest spectrum among our G-type stars, in spite of its age of $\simeq 4 \times 10^9$ years. Independent microwave observations confirm the presence of a hot and very active corona (Güdel et al. 1995) and furthermore strongly indicate the possible presence of a companion. A definite proof of the existence of a companion however, is still missing. Located in the subgiant branch, this late G-type star is a probable descendant of a mid F-type main sequence star, as deducible from theoretical evolutionary tracks. The higher mass and the more advanced evolutionary state with respect to the other stars of our sample may explain the peculiarity shown.

The very different results obtained for the two observational sequences #1 and #2 of the star GJ 559 (see Figs. 6 and 7) deserve some comments. While we can consider the time interval #1 as representative of the usual quiescent state of the moderately low-activity corona of the star, we emphasize that, although no variability, or clearly evident flare-like events were found in the light curve of the observational sequence #2, its high count rate (about a factor 2 higher than that of the observational sequence #1) might suggest the presence of hot plasma in a temporarily excited state.

4. Summary and conclusions

In the present work we have adopted the 2-T model and the loop model to fit ROSAT/PSPC spectra of G-type stars. The first in general yields good fit results but is inadequate to yield information on the stellar coronal structures. The fitting with the *one-loop* model provides, in the majority of the cases, unrealistically long loops, namely orders of magnitude larger than the stellar radius, and therefore hardly in a static configuration.

The *two-loop* model fitting provides a much better fitting and a more realistic scenario of the observed stellar coronae, suggesting the presence of two dominant loop populations in the coronae of the G-type stars: relatively cool and moderately high-pressure loops, covering a conspicuous fraction of the stellar surface, and very hot and very high-pressure loops, similar to solar flaring loops, covering only a very small fraction of the stellar surface.

As already remarked in Paper I, II and IV the temperatures derived from the 2-T model fitting are not directly comparable to the two-loop model $T_{\max}$ since the first ones are average plasma temperatures weighted with the source spectrum folded

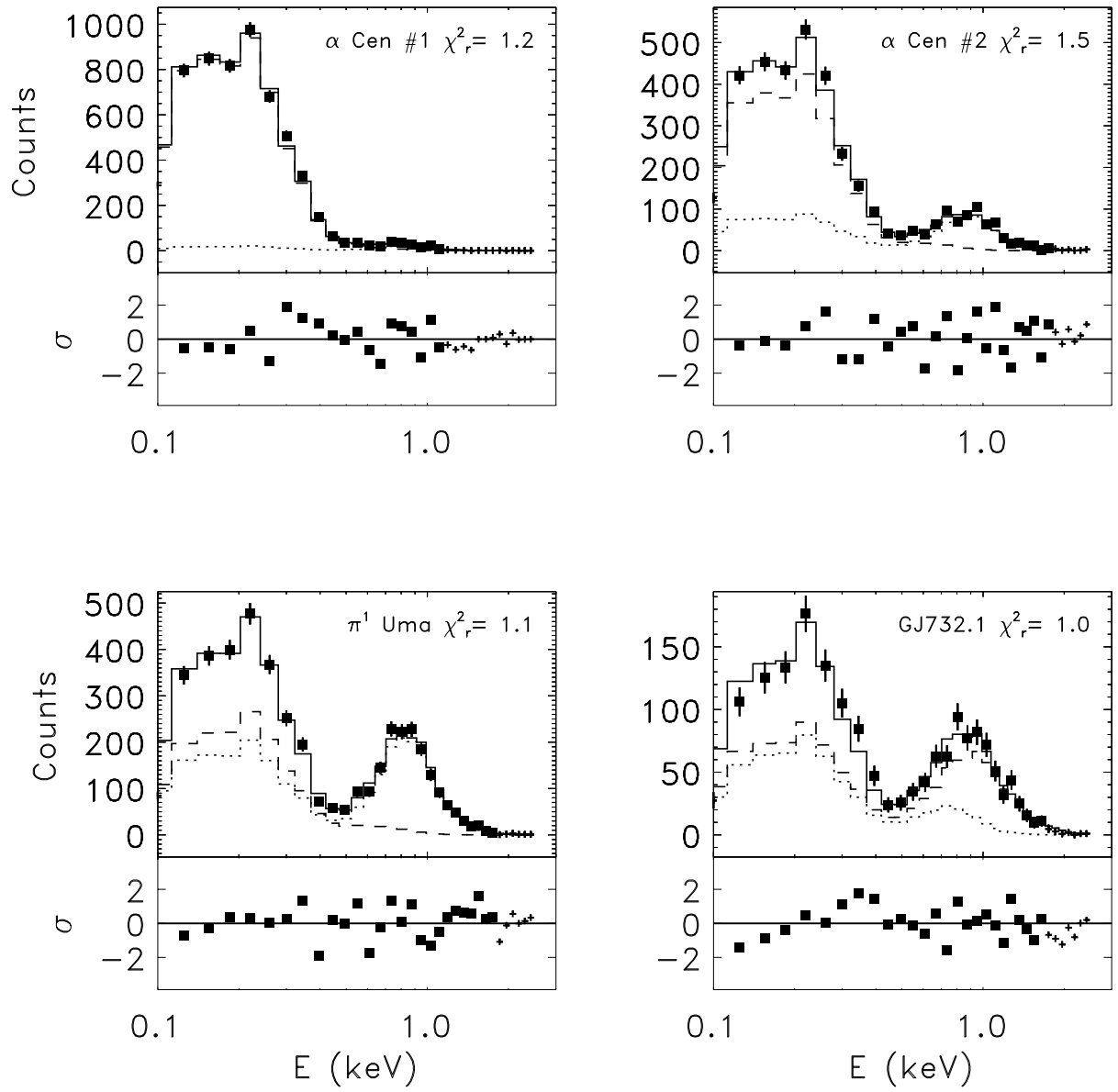

Fig. 3. ROSAT/PSPC spectra, best-fit two-loop model spectra and fit residuals for GJ 559 (α Cen) #1 OBI2 and #2, GJ 311 (π^1 UMa) and GJ 732.1. Dashed and dotted lines refer to the low-$T_{\max}$ and to high-$T_{\max}$ loop component contributions to the spectrum, respectively. The total spectrum is represented with a solid line.

with the instrument response and the second ones yield just the maximum plasma temperature inside the loops.

The loop modeling provides *indirect* evidence on the structures present in the stellar coronae as well as on the magnetic field and the coronal heating. As for the magnetic field, the loop plasma pressure obtained from the fitting allows the inference of a lower limit on the magnetic field intensity required to confine the loop plasma. The best-fit values cover a wide range, the maximum occurring for the hot component of GJ 620 #1: 2.4×10^4 dyn cm^{-2} implying a magnetic field intensity of, at least, ≈ 780 Gauss. Such a value is not too high even with respect to what measured on the Sun's surface. Since, furthermore, on very active stars there is clear evidence of strong magnetic fields, either through measurements of magnetic effects on spectral lines (Saar & Linsky 1986; Rueedi et al. 1997) or through the inference of star-spots covering a large fraction of the stars surface, our estimates of the magnetic field agree with the accepted scenario of stellar atmospheres. Such very high values of pressure, however, on the solar corona are only observed during flares.

It is worth noting that the determination of the pressure, in the loop fitting, is related with that of the filling factor as well as loop length: in particular the same X-ray flux can be achieved with relatively long, low-pressure loops covering a large fraction of the stellar surface or with shorter, high-pressure loops and a small filling factor. As for the filling factor, there appears to be a trend: the cold loop component may cover either a large or a small fraction of the star, while the hotter loop component, even

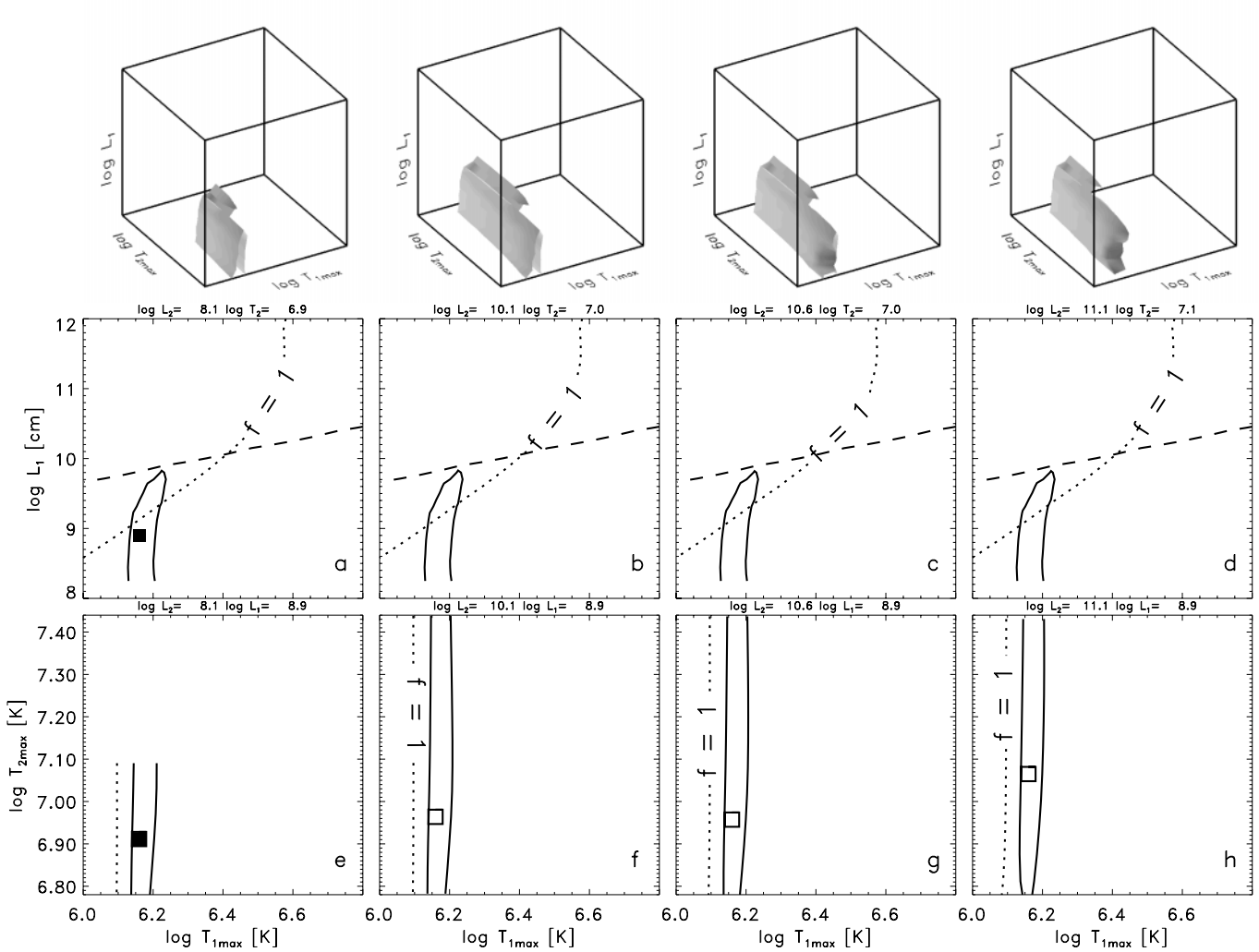

Fig. 4a–h. Two-loop model solutions. The figures in the top row show 3-D confidence regions of χ^2 at 90% level in the $T_{1\max}$ - $T_{2\max}$ - L_1 space at four fixed values of L_2, for the two-loop model analysis of GJ 559 (α Cen) #1 OBI2. The figures in the middle row show cross-sections of the corresponding 3-D confidence regions, in the $T_{1\max}$ - L_1 plane, at fixed $T_{2\max}$ values (corresponding to the minimum χ^2 location within each 3-D confidence regions also shown as a square symbol in the corresponding lower panel). In the lowest row, we show cross sections of the 3-D confidence regions, in the $T_{1\max}$ - $T_{2\max}$ plane, all at the best-fit L_1 value. The filled square marks the global χ^2 minimum, i.e. the best-fit model, while the empty squares mark the minimum χ^2 location within each 3-D confidence region.

when very luminous, occupies a relatively smaller fraction of the star's surface. The high temperature of the hotter component and the relatively small fraction of star's surface covered make such a component somehow reminiscent again of solar flares.

The above results may also provide a clue on how active stars manage to achieve higher and higher *average* X-ray surface fluxes with higher and higher activity levels: it appears that the pressure (or equivalently the luminosity per loop), and maybe also the filling factor, get higher with activity.

A particular insight comes from the analysis of the volume emission measure distribution as obtained from the best-fitting two-loop models. Comparison of our results with analogous ones obtained from two-loop model fitting of ROSAT/PSPC spectra of G-type stars in young star clusters and associations (Maggio et al. 1997b) gives a broader and more complete perspective. We find that the loop populations at lower $T_{\max}$ in our sample and in the young G-type stars analyzed by Maggio et al. (1997b) have comparable luminosities, but the higher $T_{\max}$ loop components found in the young G stars have significantly larger luminosities than the corresponding ones in the present sample. The two works show the same trend, i.e. more and more active stars show a larger and larger X-ray luminosity coming from the hotter loop component.

As for the loop geometry, the loop length of the hot component is typically unconstrained, only on the basis of the spectral fitting with loops. However if one recalls the knowledge coming from the solar case, where the hotter plasma is confined in compact loops located in active regions (Watanabe et al. 1995) and where the magnetic field is more intense and the magnetically related heating plays a bigger role, one is easily led to discard any long loop solution and consider only short and high-pressure loops. As an aside we note that on the Sun the smaller loops located in the core of active regions are also the site of more intense coronal activity (in terms of heating,

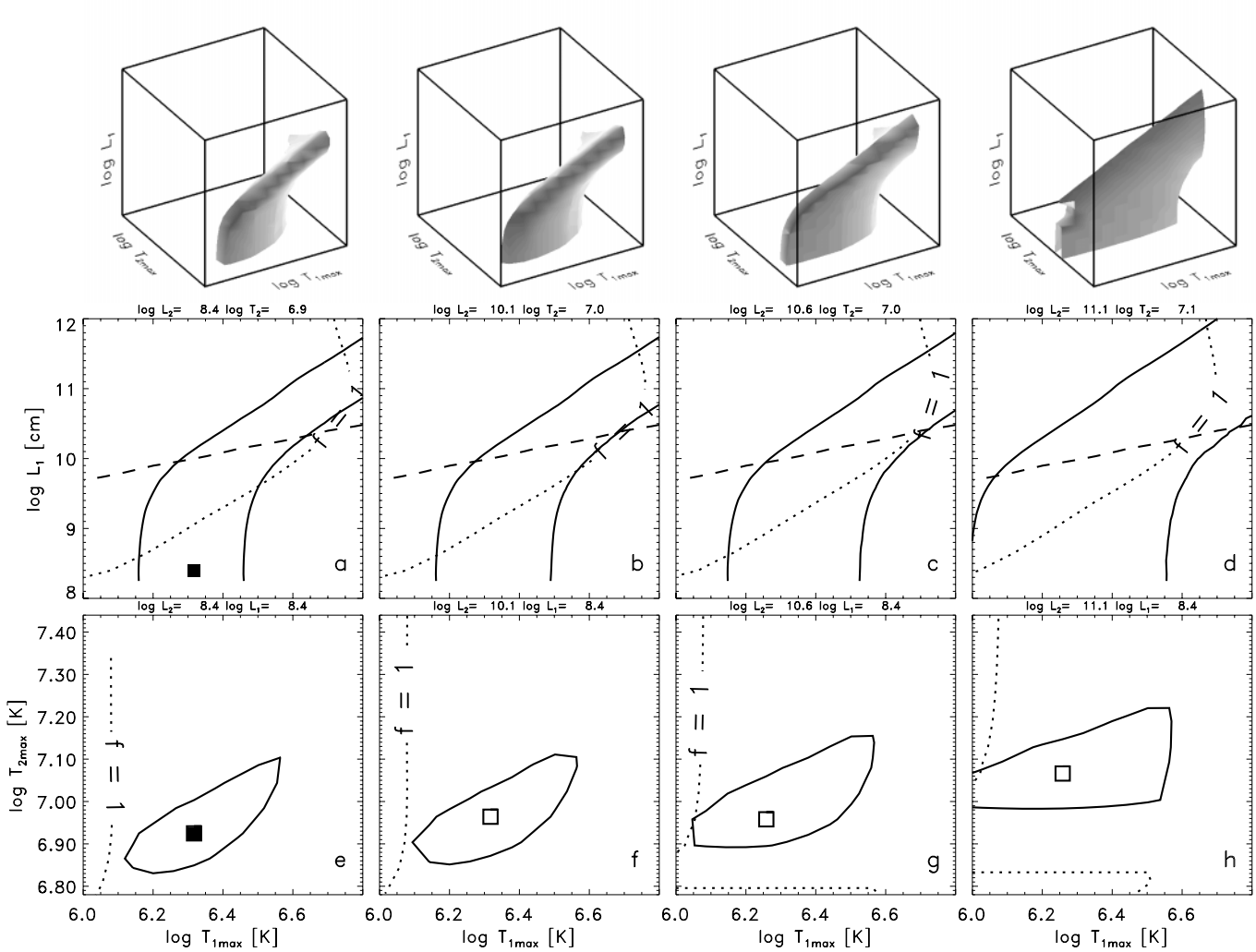

Fig. 5a–h. The same as Fig. 4 but for GJ 311 (π^1 UMa)

plasma motions, and magnetic fields) making such a hypothesis even more acceptable since these hot loop components tend to be more prominent in the more X-ray luminous stars.

However, the implications of the loop length on the heating are far-reaching. The heating per unit volume, as derived from the loop plasma scaling laws (Rosner et al. 1978) scales as $E_H \propto T_{\max}^{7/2}/L^2$. Both the high temperature and the assumption of short lengths lead to the conclusion that a very intense volumetric heating is at work in such loops. On one hand, one may imagine that they are a class of short and very hot loops in steady conditions; it remains to be understood whether the physical mechanism heating steady solar loops may be the same occurring in such much hotter loops. On the other hand, the hot loop component found in stellar coronae may be the result of a superposition of highly frequent, temporally unresolved or overlapping microflaring events (Parker 1983, 1988), hidden in the resulting light curves, which therefore do not show any large luminosity fluctuations. If the frequency of such flare-like events decreases with decreasing X-ray luminosity and age, as suggested by some authors (see Güdel et al. 1997), they do not completely overlap and luminosity fluctuations may become more evident leading to detectable variability.

The above considerations may in principle raise some doubts on the applicability of a static loop model to stellar coronae, particularly in the cases (GJ 566 and GJ 502) of evident light curve variability. However if the flaring events occur on timescales much shorter than the hydrodynamic ones, so that the emission appears nearly constant, the experience with the solar case (Kopp & Poletto 1993, Peres et al. 1993) suggests that the emission spectrum approaches the one pertaining a loop in stationary conditions, because the time scale of the evolution of plasma inside the loop is much longer than that of the heating and the latter acts effectively as if it were constant; in other words the corona behaves as if heated with a stationary heating rate. At the other extreme, very gradual flares, possibly overlapping ones, may mimic again a stationary behavior, because the plasma is in nearly hydrostatic conditions during the dominant decay phase. Some limit to the applicability of hydrostatic models may be found if we are observing the rise and the decay phase of isolated flares, which it does not appear to be the case in our data.

Such considerations on one hand show the deeper level of insight allowed by the loop model fitting, on the other hand

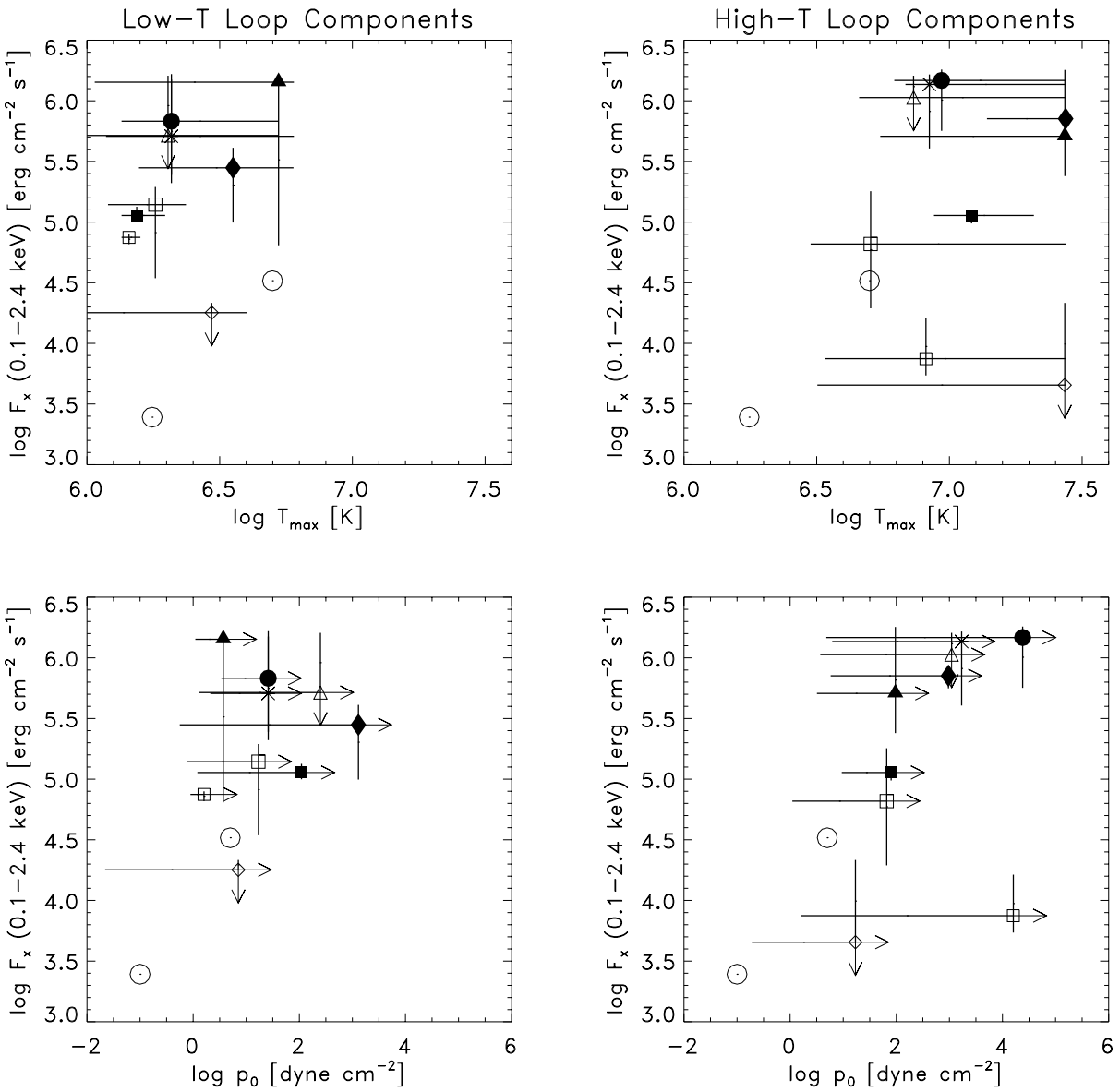

Fig. 6. X-ray surface fluxes, computed for each loop component of the two-loop model fitting, vs. $T_{\max}$ and p_0 for each star of our sample. The symbols (filled triangle GJ 17.3, cross GJ 311, square GJ 502, diamond GJ 534, filled square GJ 559 #1, square GJ 559 #2, triangle GJ 566, filled circle GJ 620.1 #1, filled diamond GJ 732.1) indicate the best-fit solutions, and the horizontal bars the range of the parameters spanned by the 90% confidence regions. The open circles mark the positions of the quiet and of the active Sun.

they lead to a challenge and a stimulus for the future observations. If the coronae of very active stars indeed contain a very active component with flares continuously occurring, as suggested by the very high heating derived for the hotter loop component, one may expect that future observations with AXAF and XMM, thanks to their very high sensitivity and spectral resolving power, may show continuous, low level, variability of the "quiescent" emission and/or of the spectrum of very active stars.

Acknowledgements. This work has made use of the SIMBAD database at CDS, Strasbourg, France. The authors acknowledge partial support from Ministero dell'Università e della Ricerca Scientifica e Tecnologica, and from Agenzia Spaziale Italiana.

References

Allen C.W. 1973, Astrophysical Quantities (3rd edition). Athlone, London
Antiochos S.K., Noci G. 1986, ApJ 301, 440
Avni Y. 1976, ApJ 210, 642
Bocchino F., Maggio A., Sciortino S. 1994, ApJ 437, 209
Briel U.G., Aschenbach B., Hasinger G. et al. 1996, ROSAT Users Handbook, on-line document at Internet nodes: "legacy.gsfc.nasa.gov" and "rosat_svc.mpe-garching.mpg.de"
Ciaravella A., Maggio A, Peres G., Serio S. 1996, A&A, 306, 553 - Paper I
Ciaravella A., Maggio A, Peres G. 1997, A&A, 320, 945 - Paper III
Demarque P., Guenther D.B., van Altena W.F. 1986, ApJ 300, 773
De Medeiros J. R., do Nascimento J. D. Jr., Mayor M. 1997, A&A 317, 701

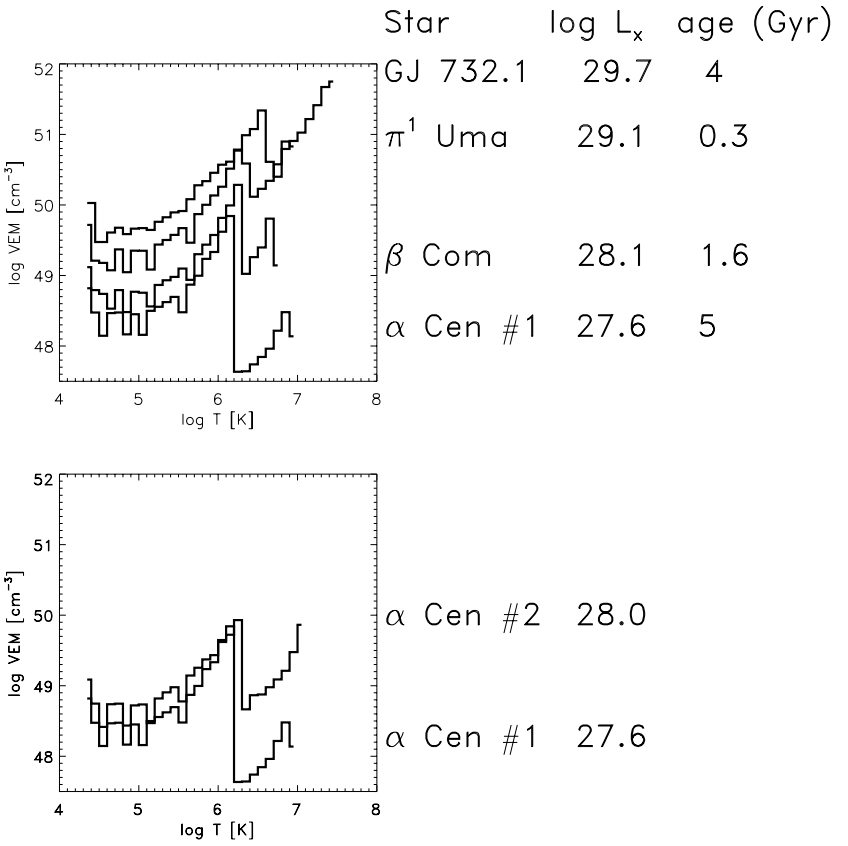

Fig. 7. Top panel: the volume emission measure distributions, vs. $\log T$, derived from the best-fit two-loop models of GJ 559 (α Cen) #1 OBI2, GJ 502 (β Com), GJ 311 (π^1 UMa) and GJ 732.1. Bottom panel: similar distributions for α Cen (GJ 559) referring to the observations #1 OBI2 and #2, whose count rates differ by a factor 2.

Donahue R.A., Saar S.H., Baliunas S.L. 1996, ApJ 466, 384
Drake S., Singh K., White N., Simon T. 1994, ApJ 436, L87
Giampapa M.S., Golub L., Peres G., Serio S., Vaiana G.S. 1985, ApJ 289, 203
Giampapa M.S., Rosner R., Kashyap V., Fleming T.A., Schmitt J.H.M.M. 1996, ApJ 463, 707
Gliese W., Jahreiss H. 1991, Bright Star Catalogue, 5th revised edition (Preliminary version, available at CDS and GSFC public data archives)
Golub L., Harnden F. R. Jr., Pallavicini R., Rosner R., Vaiana G.S. 1982, ApJ 253, 242.
Gray D. F. 1984, ApJ 281, 719
Güdel M., Schmitt J.H.M.M., Benz A.O. 1995, A&A 302, 775.
Güdel M., Guinan E.F., Skinner S.L. 1997, ApJ 483, 947.
Guenter D.B., Demarque P. 1996, ApJ 456, 798
Harrington R.S., Dahn C.C., Kallarakal V.V. et al. 1993 AJ 105, 1571
Kano R., Tsuneta S. 1995, ApJ 454, 934
Kano R.,Tsuneta S. 1996, PASJ 48, 535
Klimchuk J., Lemen J.R., Feldman U., Tsuneta S., Uchida Y. 1992, PASJ 44, L181
Kopp R., Poletto G. 1993, ApJ 418, 496
Landini M., Monsignori Fossi B.C., Paresce F., Stern R.A. 1985, ApJ 289, 709
Linsky J., Serio S. eds. 1993, "Physics of Solar and Stellar Coronae": G.S. Vaiana Memorial Symposium, Kluwer Ac. Publishers.
Maggio A., Peres G. 1996, A&A 306, 563 - Paper II
Maggio A., Peres G. 1997a, A&A 325, 237 - Paper IV
Maggio A., Reale F., Peres G., Ciaravella A. 1994, CPC 81, 105
Maggio A., Micela G., Peres G. 1997b, Mem. SaIt, Proceedings "Cool Stars in Clusters and Associations", ed. R. Pallavicini, in press
Mewe R. 1991, Adv. Space Res. 11, 127.
Morrison R., McCammon D. 1983, ApJ 270, 119
Ottmann R. 1993, A&A 273, 546
Peres G., Reale F., Serio S. 1993, in "Physics of Solar and Stellar Coronae": G.S. Vaiana Memorial Symposium, Kluwer Ac. Publishers, p. 151
Porto de Mello G.F., Da Silva L. 1997, ApJ 476, L89
Parker E.N. 1983, ApJ 264, 642
Parker E.N. 1988, ApJ 330, 474
Raymond J. C., Smith B. W. 1977 ApJS 35, 419 bibitem[] Rosner R., Tucker W. H., Vaiana G.S. 1978, ApJ 220, 643
Rueedi I., Solanki S.K., Mathys G., Saar S.H. 1997, A&A 318, 429
Saar S.H., Linsky J.L. 1986, Adv. Space Res. 6, 235
Saar S.H., Osten R.A. 1997, MNRAS 284, 803
Schaller G., Schaerer D., Meynet G, Maeder A. 1992, A&AS 96, 269
Schmitt J.H.M.M., Harnden F.R. Jr., Peres G., Rosner R., Serio S. 1985, A&A 288, 751
Schmitt J. H.M.M. 1997, A&A 318, 215
Schrijver C.J., Lemen J.R., Mewe R. 1989, ApJ 341, 484
Serio S., Peres G. Vaiana G.S., Golub L., Rosner R. 1981, ApJ 243, 288
Soderblom D.R. 1986 A&A 158, 273
Soderblom D.R., Mayor M. 1983 ApJ 402, L5
Stern R.A., Antiochos S.K., Harnden F.R. 1986, ApJ 305, 417
Voges W., Gruber R., Harbel F.et al. 1994, Rosat News No. 32
Walter F. 1982, ApJ 253, 745
Watanabe T.,Hara H., Shimizu T. et al. 1995, Sol. Phys. 157, 169
White N., Arnaud K., Day C.S.R., et al. 1994, PASJ 46, L97